Contrast amplification in global texture orientation discrimination

Lawrence G. Appelbaum Center for Cognitive Neuroscience, Duke University, Durham, NC, USA

Zhong-Lin Lu Department of Psychology, University of Southern California, Los Angeles, CA, USA

George Sperling Department of Cognitive Science, University of California, Irvine, USA

We show that adding a low-contrast texture stimulus that is far below its own detection threshold to an ambiguously oriented high-contrast texture can produce an easily perceived global orientation. When such a low-contrast (e.g., 0.1%) test texture and a high-contrast (e.g., 2%) amplifier texture are interleaved, the effective strength for global orientation detection closely approximates the product of the two contrasts. Therefore, adding two ambiguous textures, an amplifier texture at 5× its threshold contrast for global orientation discrimination and a test texture at 1/5× its threshold contrast, produces threshold global orientation discrimination, that is, 5× amplification of the below-threshold test texture. The observed 5× amplification factors are larger than facilitation effects reported in other pattern tasks. Amplification is 11× when orientation discrimination thresholds are compared to absolute detection thresholds. For second-order textures, maximum contrast amplification is about 2.5×. A contrast gain control model is presented that accounts for 90% of the variance in observed d' for texture patterns of differing geometries, exposure durations, and component contrasts. In the model, very low-contrast orientations are represented by power functions of their contrasts, with an exponent greater than two. As the contrast of an amplifier texture increases beyond about 4%, feed-forward gain control exerted by the amplifier ultimately nullifies the amplification effect and produces masking.

Keywords: contrast amplification, facilitation, texture, contrast gain control, second order

Citation: Appelbaum, L. G., Lu, Z.-L., & Sperling, G. (2007). Contrast amplification in global texture orientation discrimination. *Journal of Vision, 7*(10):13, 1–19, http://journalofvision.org/7/10/13/, doi:10.1167/7.10.13.

Introduction

Contrast amplification

The perceptual strength of a test stimulus presented to one location on the retina at any moment in time is modified by the presence of other stimuli presented superimposed on the test or in adjacent locations. Most commonly, a superimposed or an adjacent stimulus competes for processing resources and impedes (masks) detection or discrimination of the test stimulus. Here we are concerned with the less common phenomenon in which a superimposed stimulus greatly improves detection and discrimination of a low-contrast test stimulus. When a very low-contrast test stimulus produces perceptual effects that are normally produced only by higher contrast stimuli, we call the phenomenon "contrast amplification."

Dipper effect

Consider, for example, the detection of a low-contrast disk or a Gabor sine wave patch (i.e., discrimination of trials containing the test stimulus from blank trials). Detection can be often, but not always, improved by a factor of about two to four by superimposing the test stimuli on to a replica of the test stimulus, a pedestal, rather than upon a uniform neutral background (e.g., Foley & Boynton, 1993; Foley & Legge, 1981; Henning & Wichmann, 2007; Legge & Foley, 1980; Nachmias & Sansbury, 1974; Olzak & Thomas, 1991; Zenger & Sagi, 1996; although for suppressive effects, see Petrov, Verghese, & McKee, 2006). Detection enhancement by a pedestal is explained by assuming that the brain's representation of stimulus magnitude is in terms of the square of the stimulus contrast rather than by contrast directly. As the amplitude of the pedestal increases, pedestal enhancement changes to pedestal masking. The reduction and consequent increase in threshold, as a function of pedestal amplitude, is called "the dipper effect."

In this work, we are concerned with an unusual dipper effect seen in an orientation discrimination task in which the test stimulus and the pedestal, or amplifier stimulus, have no points in common. The amplifier stimulus has zero contrast wherever the test has nonzero contrast, and vice versa. We use the term amplifier stimulus (rather than pedestal) because it is appropriate considering its perceptual effect and because "pedestal" suggests a spatial

doi: 10.1167/7.10.13 Received November 16, 2006; published July 26, 2007 ISSN 1534-7362

overlap between test and amplifier, which is not the case here. (However, the mechanism by which an amplifier stimulus exerts its effect is more complex than simple contrast amplification; as precisely detailed in the accompanying model.) The particular texture stimulus used here (Figure 1a, left) to study contrast amplification in global orientation detection is a texture analog of a similar stimulus previously used to study direction discrimination in a motion paradigm (van Santen & Sperling, 1984). The advantage of this stimulus is that it has a unique property (the product rule) that makes it particularly useful in discovering the underlying mechanism and that it already has received a great deal of study in the motion domain (Lu & Sperling, 2001a; van Santen & Sperling, 1984).

Product rule

Consider the stimulus illustrated in Figure 1a. The even rows have contrast m_e and the odd rows have contrast m_o; successive rows are shifted 90° rightward. As a motion stimulus (right), successive rows represent stimuli at successive instances of time. The progression from top to bottom represents global motion from left to right of a grating in which successive frames alternate between low and high contrast. The same stimulus (left), simply viewed as a static texture pattern (rather than as a representation of motion), has a global slant orientation from upper left to lower right.

van Santen and Sperling (1984) proved that when a Reichardt model (Figure 1b) was presented with this type of motion stimulus, the model's output was proportional to the product of the contrasts of the even and the odd frames, $m_e \times m_o$. This product rule also holds for the equivalent motion energy model (Adelson & Bergen, 1985). Empirical tests with motion stimuli of temporal frequencies 1.8 and 12.5 Hz showed that the product rule holds in the following sense: All the different combinations of contrasts of m_e and m_o that had the same product ($m_e \times m_o$) produced the same motion discrimination accuracy, provided the contrast of the higher contrast grating was not above 8.5% (van Santen & Sperling, 1984). Subsequently, Werkhoven, Sperling, and Chubb (1994) found the product rule to hold for second-order

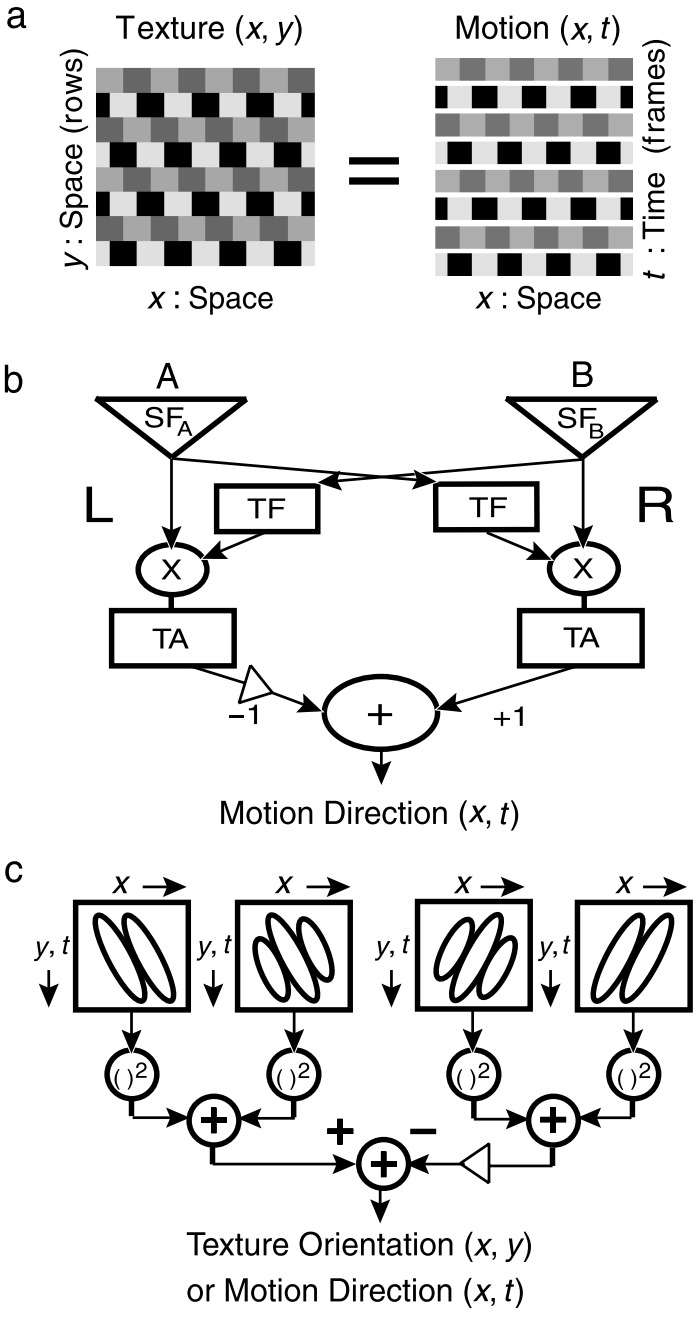

Figure 1. Motion direction and texture orientation mechanisms: (a) Motion texture equivalence when similar square-wave gratings translate 90° between successive texture rows (left) or motion frames (right). When rows are successively presented in space, the display represents a slanted texture. When the frames are successively presented in time, the display represents rightward apparent motion. The product rule (model output-amplitude proportional to $m_e \times m_e$) applies to both the motion and the texture version of this stimulus configuration. (b) Schematized elaborated Reichardt detector proposed to underlie human visual motion perception. SF indicates a spatial filter, TA indicates a temporal delay filter, × indicates multiplication, and TA indicates a temporal averaging filter. A positive output indicates motion from left to right; negative outputs indicate the opposite direction. (c) Motion (or texture) energy model. The two adjacent ellipses represent a cosine filter, the three adjacent ellipses represent a sine filter; the cosine and sine filter are a quadrature filter pair of the type proposed for determining texture-slant (Knutsson & Granlund, 1983) and motion direction discrimination (Adelson & Bergen, 1985). The squared outputs of the left quadrature filters are summed and then subtracted from the squared, summed output of the right quadrature pair. A positive output indicates motion from left to right or, equivalently, a slant from upper left to lower right. Negative outputs indicate the opposite. For an appropriate choice of filters, models b and c produce equivalent outputs.

motion stimuli. Lu and Sperling (2001a, 2001b) further capitalized on the "product rule" in their development of a sensitive calibration procedure in motion perception. They realized that when the contrast of one component of a stimulus was raised, the other could be lowered far below its own threshold and yet, according to the product rule, the combination would still be detectable.

Deriving $m_e \times m_e$ from quadrature

The product rule (motion strength is proportional to $m_e \times m_e$) is a consequence of the fact that the Reichardt model (due to its multiplier elements) and the motion energy model (due to its quadrature detectors) have outputs that are proportional to the squared amplitude of Fourier motion components. Even prior to these motion detection models, computational models of texture orientation pioneered the use of quadrature detectors. For example, in their computational model for detecting the orientation of texture gratings, Knutsson and Granlund (1983) used quadrature filters identical to those of the motion energy model illustrated in Figure 1c to extract orientation energy in x, y space.

The product rule ($m_e \times m_o$) can be easily derived heuristically from quadrature Fourier considerations. In a quadrature model for deciding between two texture orientations (or two motion directions), the squared amplitude sine wave in one orientation is compared to (i.e., subtracted from) the squared amplitude of the sine wave in the mirror opposite orientation. In our texture stimuli, the amplitudes of the sine waves being compared can be estimated from Figure 2a, where two lines are shown that trace the minimum points of the fundamental sine wave representing the upper-left-to-lower-right orientation. Relative to the background (mean gray), the average value of the minimum along this path is $-(m_e + m_o) / 2$. Similarly, the average value of the sine wave maximum along a path between the two black lines is $+(m_e + m_o) / 2$. Thus, the amplitude of this sine wave is proportional to $(m_e - m_o)$. The amplitude of the mirror opposite sine wave is proportional to $(m_e - m_o)$. The squared difference between these two amplitudes is proportional to $m_e \times m_o$, the product rule.

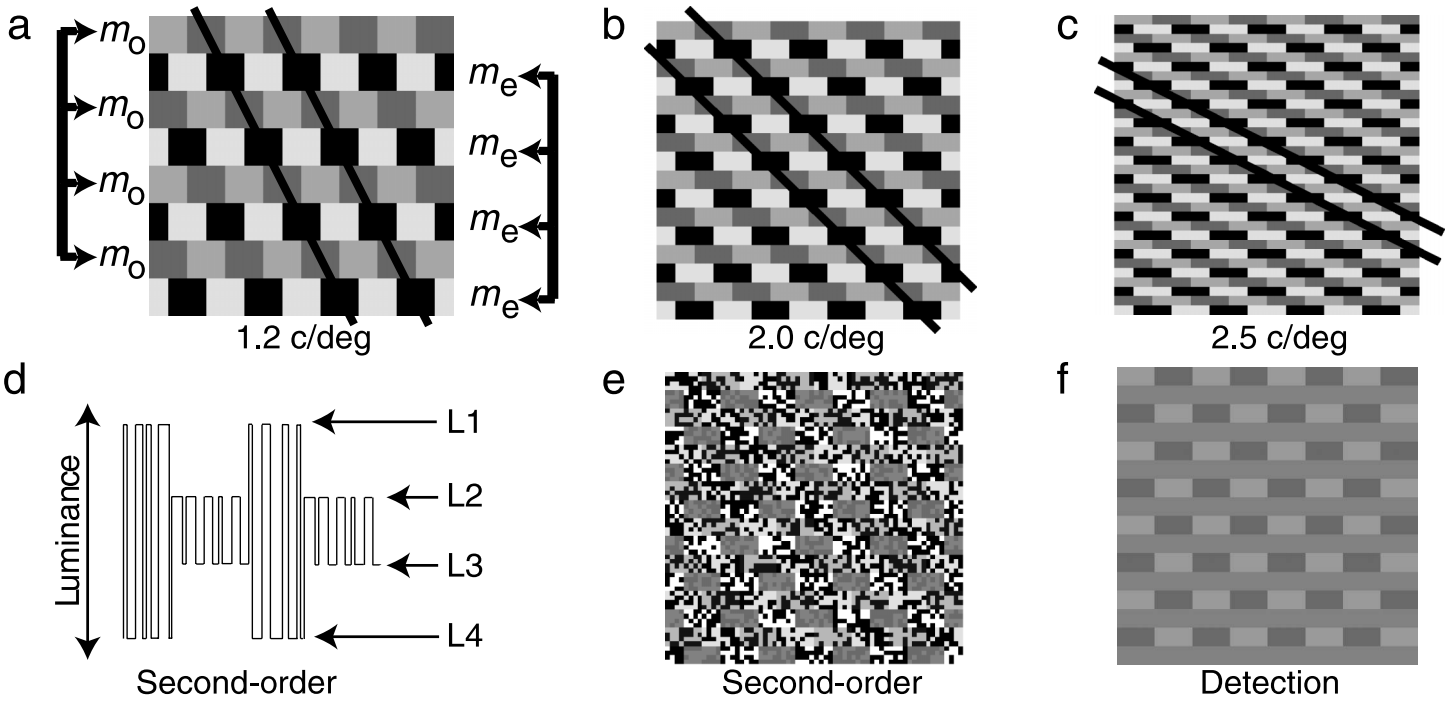

Figure 2. Representative texture stimuli and the spatial frequency of the global texture orientation at the viewing distance of 94 cm. (a) 1.2 cpd texture oriented at +22.5° off vertical. (b) 2.0 cpd texture oriented at +45° off vertical. (c) 2.5 cpd texture oriented at +67.5° off vertical. (Note: The contrast has been dramatically increased for illustrative purposes.) Spatial frequency and orientation are indicated by bars spaced one cycle apart (not included in actual display). There are two possible texture orientations, the one depicted (e.g., +22.5° and its mirror opposite −22.5°). Observers are instructed to indicate the orientation with a button press. Panel a illustrates the construction of sandwich displays. Even row contrast modulations are labeled m_e. Odd row contrast modulations are labeled m_o. (d) A schematic luminance profile of a single horizontal row of the second-order, contrast-modulated stimulus. (e) A 2.0-cpd contrast-modulated texture designed to stimulate a second-order orientation detection system. Second-order textures were tested in a separate sessions from first-order textures. (f) The detection stimulus that was tested in separate sessions. The detection stimulus is identical to a 2.0-cpd discrimination stimulus (e.g., panel b) with the even row contrast $m_e = 0$. The observers' task was to detect the presence of the odd rows (the texture) that were present on half the trials.

The formal equivalence of detecting motion direction and global texture orientation

The problem of determining the direction of motion in a one-dimensional sampled motion display is formally equivalent to the problem of determining the slant of a two-dimensional texture grating (Adelson & Bergen, 1985). As demonstrated by Adelson and Bergen (1985), front-end receptive fields can be interpreted either as the space–time filters of motion detectors (Figure 1b or 1c) or the space–space filters of texture detectors (Figure 1c). Here we exploit this equivalence in the construction of our stimuli. Figure 1a illustrates how the $x - t$ space–time profile of a rightward motion display translates into the $x - y$ space–space profile of an oriented texture display. When individual frames are successively presented in time, the 90° phase shift of the gratings is seen as a rightward motion. When the gratings are successively presented as rows in space, the phase shift is seen as a texture slant.

The multiplicative rule in motion perception (and in computational models of motion) may well generalize to global orientation detection in texture perception. Thus, when the contrast of one set of rows, say the even rows, is high, the contrast of the odd rows can be quite low while performance in global orientation discrimination remains constant. Following this logic, there should be texture displays in which the odd rows are well below threshold of detection and yet they support accurate judgments of global orientation. However, in motion perception, when element contrasts become too high, contrast gain control (Lu & Sperling, 1996) becomes significant, and the strict multiplicative rule breaks down, a property that should hold as well for static textured stimuli.

The plan

In this study, we investigate contrast amplification in texture perception over a wide range of spatial and temporal configurations to find the optimal conditions for perceptual facilitation and to determine the limits of facilitation, that is, where masking begins to dominate. A contrast gain control model of orientation discrimination will be proposed to account for the experimental data and to show how the computations that support orientation discrimination naturally arise in a more general model of perceptual processing.

Methods

Observers

Three observers participated in this experiment. All observers had 20/20 or corrected to 20/20 vision, and informed consent was obtained for each participant in accordance with the institutional human subjects policy. All three observers were tested on the main discrimination task, whereas two of the observers were also tested with a separate second-order discrimination task (Subject 1 [S1] and Subject 3 [S3]) and a separate control detection task (S1 and Subject 2 [S2]).

Procedure

The main discrimination task used a two-alternate forced-choice design, in which observers made orientation discriminations on individual texture patches. Each patch was aligned in one of two orientations, either upper left to lower right or upper right to lower left. Observers fixated on a small cross in the center of the screen initiated each trial, and following the stimulus presentation, they indicated the orientation with a button press. Auditory feedback was provided following each trial.

Stimuli

Stimuli were generated on a Power Macintosh 8600/250 running Psychtoolbox (Brainard, 1997; Pelli, 1997) and were presented on a monochrome monitor with a frame rate of 120 Hz, with an interface that yielded 6144 levels of intensity (12.6 bits). The mean luminance level was 40 cd/m^2. Texture patches subtended 4.25° × 4.25° were centrally presented and were viewed from a distance of 94 cm. A head mount was employed to reduce unwanted head movements.

Individual texture patches were constructed of vertically "sandwiched" rows composed of luminance-modulated square-wave gratings. All rows had the same period, with successive rows translating 90° in a consistent direction. Figure 2a illustrates the construction of a single stimulus texture patch. In these stimuli, the odd and even row contrasts were independently manipulated of each other. Even row contrast modulations are labeled as m_e, and odd row contrast modulations are labeled as m_o. An important property of this type of display is that successive even rows or successive odd rows translate 180° out of phase. When considered alone, neither even rows alone nor odd rows alone yield information about the orientation of the texture. Texture orientation can be determined only by integrating the even and the odd rows.

In the main experiment, each block of trials consisted of two types of randomly intermixed patches. In one of these types of patches, referred to as the ordinary threshold condition, the contrast of the odd and even rows were equated ($m_e = m_o$). These trials were presented at contrasts ranging from 0.1% to 1%, and the method of constant stimuli was used to determine the contrast amplitude that produced 75% probability ($d' = 1.36$) of correct texture orientation judgment. The ordinary threshold

condition serves as the reference for orientation discrimination of textures with unequal even and odd row contrasts ($m_e \neq m_o$).

In the other type of patches, one of four different contrasts, 1%, 2%, 4%, and 8%, was presented in the even rows, whereas the odd row contrasts were lowered to determine threshold for orientation detection ($m_e > m_o$). The method of constant stimuli was again used to determine the odd row (m_o) contrast that produced 75% correct texture orientation judgment for each of the four fixed contrasts of the even rows. We refer to the even rows as amplifier rows and the odd rows as test rows. All conditions were randomized within each individual session. A session contained 500 trials; five levels of m_e and five levels of m_o, with 20 trials of each (10 for each orientation).

To test the properties of amplification over a broad range of conditions, three different display durations and three different geometrical configurations were employed. Individual stimulus durations were 50, 100, or 250 ms. The three geometric configurations tested were made by adjusting the vertical height of each grating row. This produced textures of 1.2, 2.0, and 2.5 cycles per degree (cpd), with orientations of ±22.5°, ±45°, and ±67.5° off vertical (Figures 2a, 2b, and 2c). The width of each cycle was fixed at 1.06° of visual angle, whereas the height of each row varied across configurations. Within an individual block of trials, geometry and display duration were kept consistent. Block order was counterbalanced.

Second-order textures

A second-order texture orientation discrimination task was conducted in a separate session with two of the observers (S1 and S3). The second-order task was identical in procedure to the 100-ms duration, 2-cpd condition in the main experiment, except that the individual amplifier and odd rows were composed of contrast-modulated texture elements. The second-order stimuli (Figure 2e) were constructed from a two-dimensional binary random noise pattern, defined at each point as $R(x, y)$, that was multiplied with a contrast-modulated square-wave envelope of the same dimensions as the luminance-modulated square-wave gratings of the main experiment. In these stimuli, $R(x, y)$ is a random variable that assumes values +1 and −1 with equal probability, independently at each spatial location x,y, with each noise element subtending 2 × 2 arcmin. Figure 2d depicts the luminance profile of these stimuli along a portion of a single horizontal row. As can been seen, the luminance profile of the noise pattern modulates between successive high- and low-contrast patches. The modulation of the gratings contrast envelope is therefore defined as the texture contrast of high-contrast stripe minus the texture contrast of low-contrast stripe divided by the average texture contrast:

$$\text{Modulation} = \frac{(L1 - L4) - (L2 - L3)}{(L1 - L4) + (L2 - L3)} \times 100\%, \quad (1)$$

where L1, L2, L3, and L4 are the pixel luminance values in the stimulus.

As in the main experiment, the modulation depths of the odd and even rows were manipulated separately and independently of each other. Even row modulations are labeled as m_e, and odd row modulations are labeled as m_o. Ordinary threshold modulations ($m_e = m_o$) were 1%, 2%, 3%, 4%, and 5%. Modulation amplitudes of the even rows (amplifiers) were 4%, 8%, 16%, and 32%. Prior to experimentation, the stimulus monitor was set for luminance linearity and all individual second-order rows underwent a black–white calibration to remove unwanted first-order contaminations resulting from black–white perceptual asymmetries (for a full description of this calibration procedure, see Lu & Sperling, 2001a, 2001b).

In these stimuli, the texture contrast modulation is a pure second-order stimulus: Its expected luminance is the same everywhere. Therefore, its texture energy cannot be determined by a conventional quadrature detector (as illustrated in Figure 1b) because the Fourier components are uninformative. However, a nonlinearity such as a full-wave rectification occurring prior to the quadrature computation could expose the oriented energy of the stimulus (for explanation of an equivalent architecture in motion displays, see Chubb & Sperling, 1988).

Detection task

A separate detection task was conducted with two of the observers (S1 and S3). The stimulus in this detection task was similar to the stimulus in the discrimination task composed of 2.0° gratings presented for 100 ms. The detection task differed from the discrimination task in that even row contrasts were set to zero (see Figure 2f). On half of the trials, the odd rows were presented at one of fifteen contrast levels. On the other half of the trials, the odd rows have 0% contrast and the display remained a mean luminance gray. Observers were instructed to indicate if the target was present through a button press and auditory feedback was given to indicate correct detection.

Estimating threshold m_o values and m_o as a function of m_e

Test row (m_o) contrast values that produced 75% correct orientation discrimination for each amplifier were derived from least squares fits to the psychometric

functions—performance (d') against odd row contrast. For all fits, psychometric functions were constrained to go through the point (0, 0) because at zero contrast (or zero modulation) the odd row textures contain no intrinsic luminance variations that could be used to support an orientation judgment. In addition, fits were not computed for accuracies greater than 95% (d' = 3.3) because those data were too unreliable.

The psychometric function for each amplifier contrast was fit with linear functions. Ordinary threshold data were fit with a quadratic function ($d' = \alpha \times m_o^2$) because in this condition both the odd and even row contrasts varied concurrently. A 75% threshold discrimination value was extrapolated for each amplifier at each of the five test contrast values tested.

Results

Figure 3a shows the psychometric functions and fits for each participant viewing textures of 2.0 cpd presented for 100 ms. In each plot, the data and fits are plotted as d' performance against test row contrast (m_o). Each fitted line indicates the d' value for a single amplifier contrast (m_e) over the range of odd row contrasts tested (m_o). The linear fits are for each of the four fixed values of m_e, whereas the ordinary threshold condition is fit with a square function.

In each plot, the threshold performance defined as d' = 1.36 or 75% correct is indicated with a solid black horizontal line. Threshold performance values for each

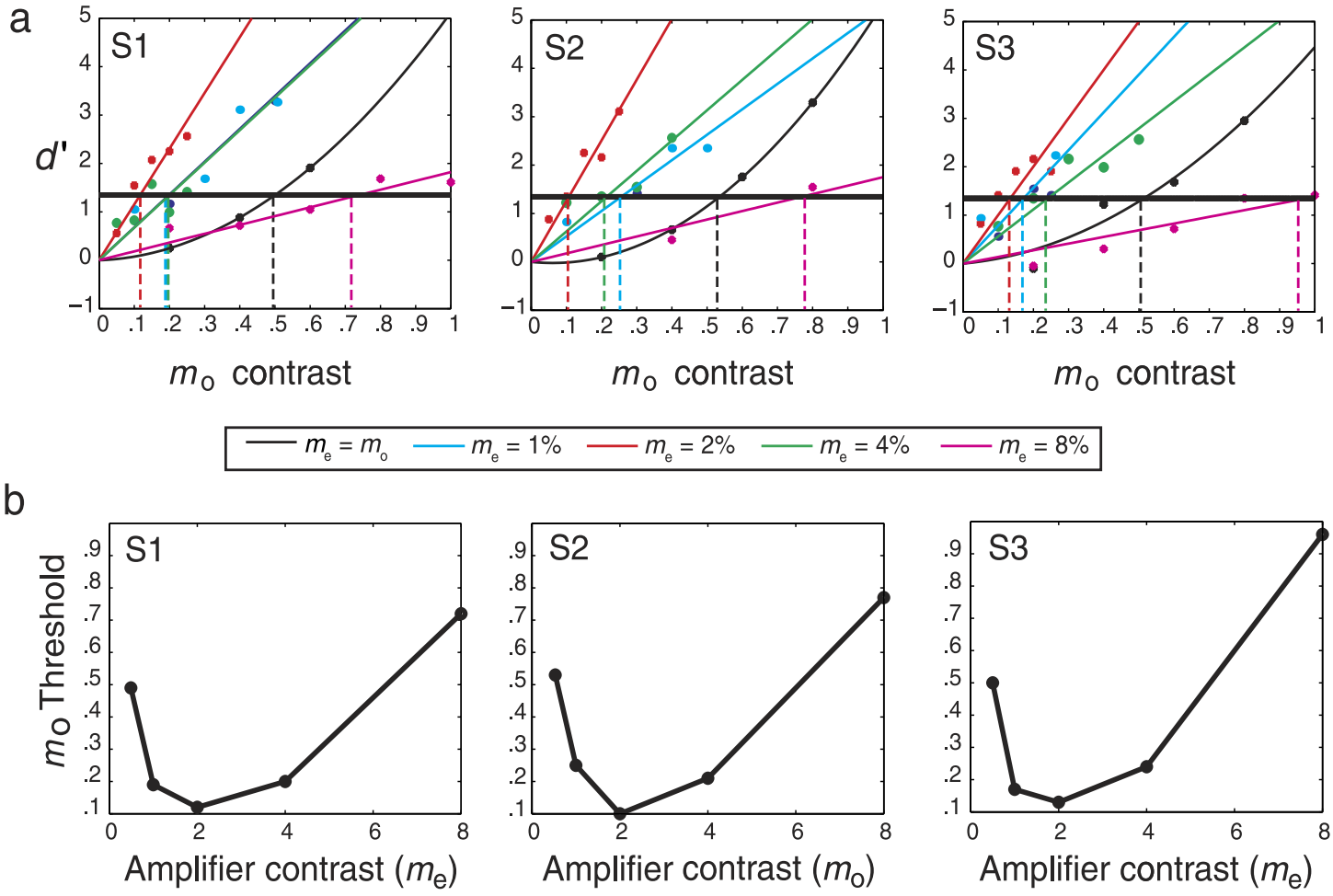

Figure 3. Experimental results for each participant viewing the 2.0-cpd textures presented for 50 ms. The top row (a) shows psychometric functions' data points, fits, and threshold interpolations for each observer. In each plot, d' for global orientation discrimination is plotted against odd row contrast modulation; m_o. All data obtained with a particular amplifier contrast modulation m_e are shown in the same color, as indicated in the middle, horizontal insert. Ordinary threshold ($m_e = m_o$) data points are fit with a square function. All others, data are fit with linear functions. The solid black horizontal line indicates the threshold detection criterion (75% correct, d' = 1.36). Vertical lines indicate extrapolated odd row contrast modulation (m_o) at detection threshold for each amplifier contrast value (for numerical values, see Table 1). (b) Graphical representations of amplifications for each observer. Threshold contrast values (m_o) for odd rows are plotted as a function of amplifier contrast (m_e). The far left point on each graph is the ordinary threshold contrast, values on the curve below ordinary threshold represent contrast amplification.

fit are extrapolated (vertical dashed lines) and listed in the third column of Table 1. These values represent the test row contrast required to maintain 75% correct performance as the amplifier contrast is varied.

To illustrate the strength of amplification, a graphical depiction is shown for each of the three observers on textures of 2.0 cpd presented for 100 ms in Figure 3b. In these plots, contrast values that produce 75% threshold performance are plotted as a function of amplifier contrast. In each case, the odd row contrast required for 75% threshold performance is approximately 0.5% contrast in the ordinary threshold condition, but only about 0.1% when interleaved with a 2% contrast amplifier. For amplifier contrast above 2%, there is a steady increase in the test row contrast required to maintain threshold performance. This function relating test row contrast to amplifier contrast is similar to the classical dipper-shaped function, a topic to which we will return later.

To arrive at a description of amplification that is independent of any theory, it is useful to describe amplification simply as the ratio of two measurable thresholds, m_o: the ordinary threshold ($m_o \mid m_o = m_e$) divided by the threshold contrast of the odd rows ($m_o \mid m_e$). This amplification factor provides an indicator of the relative contrast of test rows when not amplified to odd rows when amplified:

$$\text{Amplification factor} = \hat{m} = \frac{(\hat{m}_o | m_o = m_e)}{(\hat{m}_o | m_e)}. \quad (2)$$

Psychophysical results from all three observers showed a consistent pattern of increasing amplification for amplifier m_e up to 2% contrast that then decreases at higher amplifier m_e values. Contrast amplification greater than one was found in all geometries and display durations. Typical maximum amplification was found to be a factor of four to five and always occurred for amplifier contrast m_e = 2%. Amplification factor values are listed in the fourth column of Table 1.

Amplification as a function of geometry and duration

Performance data for the full range of geometries and display durations tested are depicted in Figure 4 for two subjects (S1 and S2). Figure 5 illustrates facilitation over all of these conditions. The pattern of increasing amplification up to a maximum at 2% holds in all condition tested for both observers. When subjects were given longer time to view texture patches (100 and 250 ms), discrimination thresholds were reduced. This increase in sensitivity is illustrated by the reduction in shaded area for longer display durations in Figure 5. No effect of geometry was seen.

Texture energy

According to the multiplicative product rule described earlier, the strength of global texture orientation is defined as the product of the component contrasts: the even row contrast times the odd row contrast ($m_e \times m_o$). If the product rule holds, it should be the case that texture displays with equal energy yield equal discrimination performance. As is done for motion stimuli (Lu & Sperling, 2001b), we define root mean square (RMS) texture energy as the square root of the product of the

Subject	Configuration	m_e	m_o	Amplification factor	RMS energy
1	$m_e = m_o$	0.49	0.49	1	0.49
m_e = 1%	1	0.19	2.58	0.44	
m_e = 2%	2	0.12	4.08	0.49	
m_e = 4%	4	0.20	2.45	0.89	
m_e = 8%	8	0.72	0.68	2.40	
2	$m_e = m_o$	0.50	0.50	1	0.50
m_e = 1%	1	0.17	2.94	0.41	
m_e = 2%	2	0.12	4.08	0.49	
m_e = 4%	4	0.24	2.08	0.98	
m_e = 8%	8	0.96	0.52	2.77	
3	$m_e = m_o$	0.53	0.53	1	0.53
m_e = 1%	1	0.25	2.12	0.50	
m_e = 2%	2	0.10	5.30	0.45	
m_e = 4%	4	0.21	2.52	0.92	
m_e = 8%	8	0.77	0.69	2.48	

Table 1. Stimulus contrasts, amplification factor, and root mean square (RMS) energy are shown for all three observers viewing 2.0 cpd textures presented for 100 ms. Stimulus row contrasts are listed in columns 2 and 3, threshold extrapolations in column 4, amplification factors in column 5, and stimulus RMS energy in column 6.

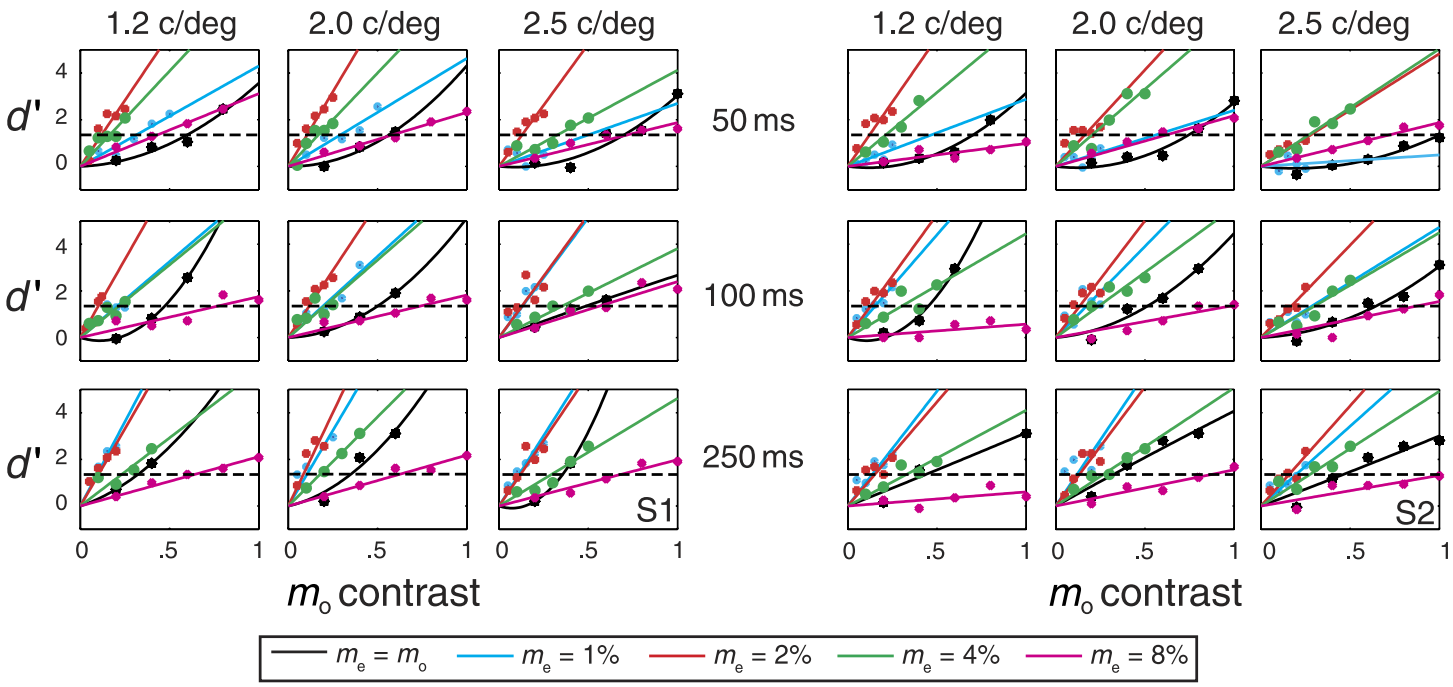

Figure 4. Accuracy of global orientation discrimination (d') as a function of test stimulus contrast m_o for four amplifier contrasts m_e and for $m_e = m_o$ (ordinary threshold). Data points and fits for observers S1 (left) and S2 (right) represent all first-order texture stimuli and conditions.

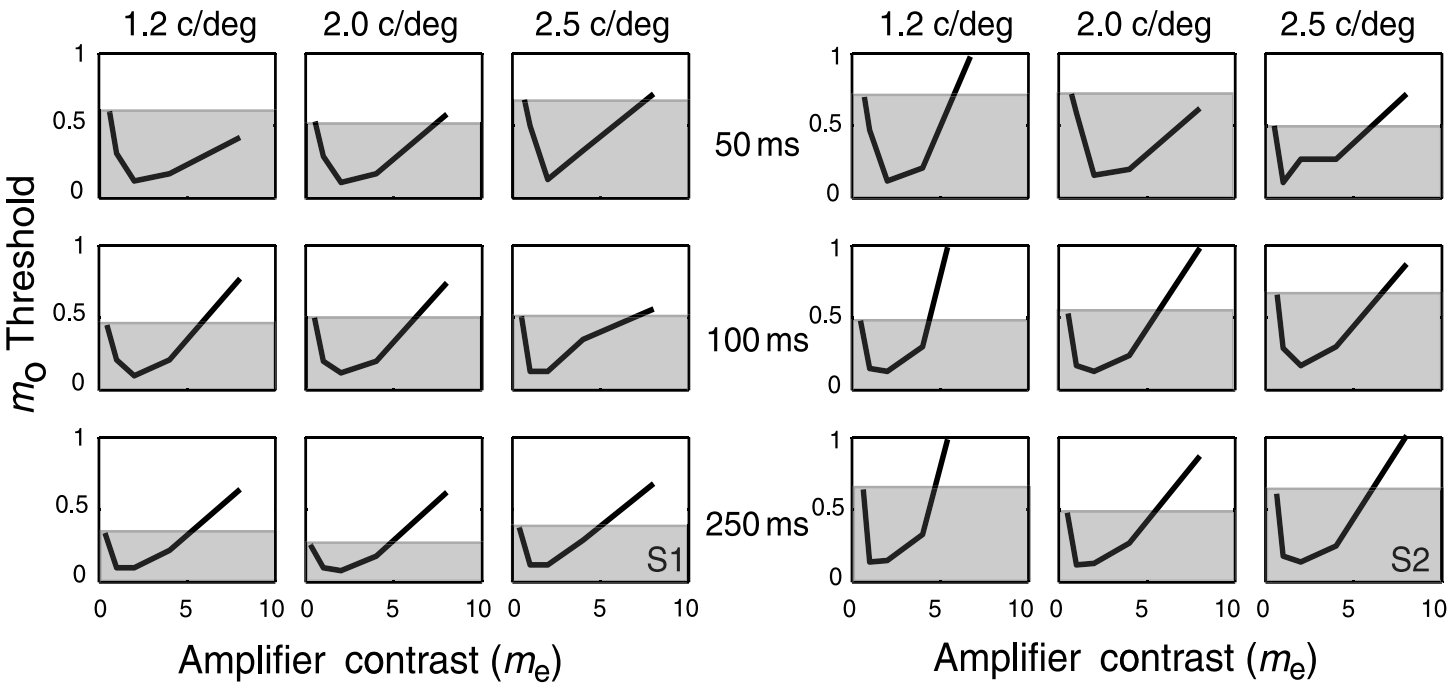

Figure 5. Graphical depiction of amplification: Plotted are dipper functions for observers S1 (left) and S2 (right) on all conditions. Threshold contrast values for test rows (m_o) plotted as a function of amplifier contrast (m_e). The shaded region in each figure indicates the relative ratio of facilitation (shaded) to masking (unshaded). Discrimination thresholds are reduced for longer display durations (reduction in shaded area).

amplifier contrast modulation times the test contrast modulation (RMS global orientation energy):

$$\text{RMS energy} = \sqrt{m_e \cdot m_o}\ . \quad (3)$$

Equation 3 is easily understood in terms of the Fourier sine wave components of the stimulus. The stimulus is specified in terms of the contrast modulations m_e and m_o for the even and the odd rows. To relate m_e and m_o to sine wave amplitudes, we refer to Figure 2a. Consider the major orientation direction. Along the dark stripes in Figure 2a (indicated by diagonal lines), the average point contrast is $-1/2(m_e + m_o)$. Along the adjacent light stripes, the average point contrast is $1/2(m_e + m_o)$. The amplitude of modulation of the major orientation direction is the average of these: $1/2(m_e + m_o)$. By similar reasoning, the amplitude of modulation of the mirror opposite (minor) orientation direction is $1/2(m_e - m_o)$. To measure the discriminability of the major and the minor orientations, the modulation amplitude of each orientation direction is squared; subtracting the minor squared amplitude from the major yields the product relation $m_e m_o$ of Equation 3.

To a first approximation, RMS energy is constant until a critical amplifier contrast is reached at which point, masking by the amplifier becomes significant, and RMS energy rapidly increases with amplifier contrast. An interesting secondary finding here is that RMS energy required to make orientation discriminations at the threshold actually reduces slightly in the range of greatest amplification. This reduction in energy is seen as the dip in the RMS curves in Figure 6 and is indicative of a slight violation of the strict product rule. This violation, although slight, is seen in all conditions. The RMS values for all three observers are listed in the fifth column of Table 1.

Comparison with control detection task

Contrast facilitation has been typically cast in light of the advantage gained in discrimination between a target and a masker relative to the absolute threshold of detection for the target in isolation (Foley & Legge, 1981; Legge & Foley, 1980). Although our amplification factor offers an index of facilitation within the constraints of our discrimination task, it is useful to also compare discrimination performance (orientation derived from the integration of m_e and m_o) to that of the detection alone (m_o). Recall that in these stimuli, successive even rows or successive odd rows translate 180° out of phase and individually offer no information about the orientation of the texture. Thus, to compute orientation, observers must detect and integrate between rows to arrive at a global orientation. Figure 7 shows detection performance as a function of contrast when the test (m_o) patches are presented in isolation against a uniform mean luminance

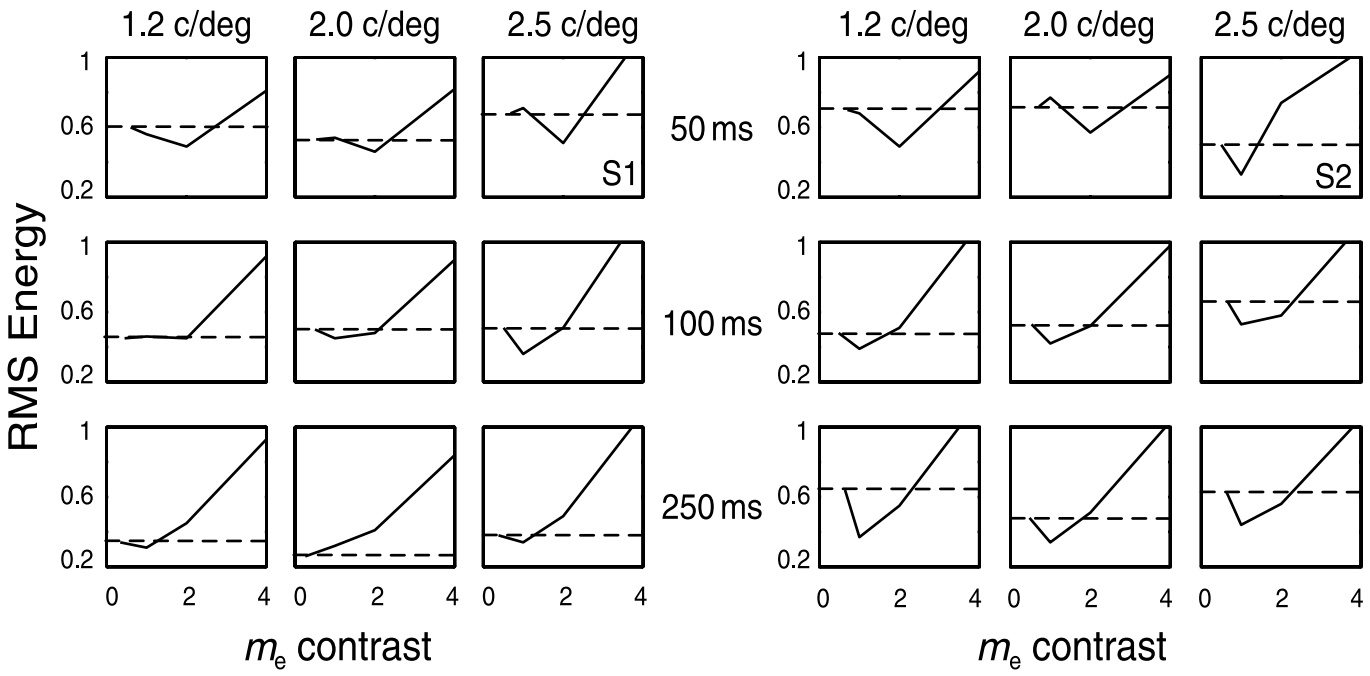

Figure 6. Root mean square (RMS) energy at threshold: Plot of RMS energy for observers S1 (left) and S2 (right) on all conditions. RMS energy at threshold performance is plotted as a function of amplifier (m_e) contrast for values up to 4%. In many of the conditions, the RMS energy required to make orientation discriminations at the threshold actually reduces over the range of greatest amplification (1–2%). This reduction in energy is seen as the dip RMS curves. Constant RMS energy (as predicted for the multiplicative property of motion) is indicated by the dashed line. A reduction in threshold energy indicates an increase in efficiency of the visual system.

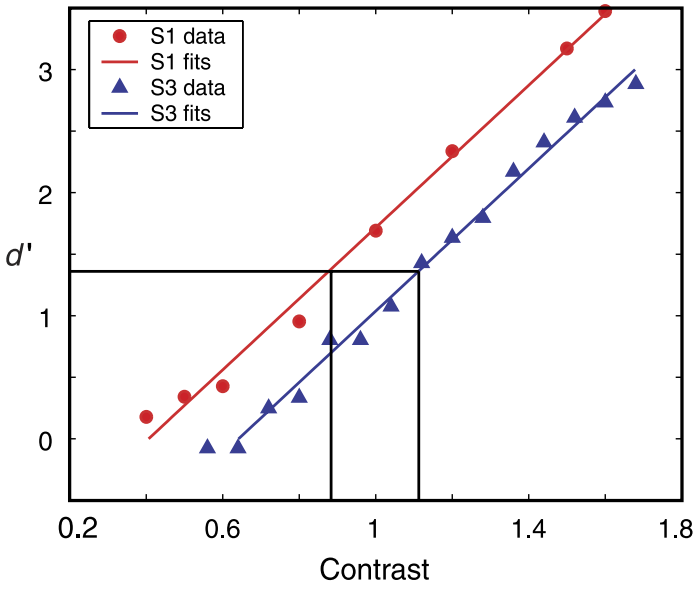

Figure 7. Control task performance: Accuracy of detecting the presence versus absence of odd stimulus rows (d') as a function of their contrast m_o when even stimulus rows have contrast $m_e = 0$. Only the test rows are presented against a mean luminance background, data (d') are shown for observers S1 and S3. Least squares fits are indicated by solid lines and extrapolated threshold values ($d' = 1.36$) are indicated by the vertical black lines. Both observers' detection thresholds (S1 0.89%, S3 1.13%) are many times greater than their global orientation discrimination thresholds in the maximally amplified discrimination task (S1 = 7.4×, S3 = 11.3×) and nearly twice as great as their threshold for ordinary global orientation discrimination (S1 = 1.8×, S3 = 2.1×).

background versus the background alone. Data are fit with a linear function, and threshold contrast values (75% correct, $d' = 1.36$) are extrapolated (black solid lines).

S1 requires 0.89% contrast for 75% threshold performance in the detection task, whereas S3 requires 1.13% contrast. These detection threshold levels are many times greater than thresholds for discrimination in the maximally amplified conditions of our main experiment (S1 7.4×, S3 11.3×).

Second-order amplification

Measurements of amplification in second-order textures produced results similar to those with first-order textures. Figure 8a depicts the psychometric functions and fits for two observers on second-order textures of 2.0 cpd presented for 100 ms. Each fit indicates the d' value for a single amplifier row of modulation (m_e) over the range of test row contrasts tested (m_o). Amplifier and test contrast modulations for the second-order textures are listed in the first two columns of Table 2. For both observers, second-order textures required greater modulations than first-order textures for equivalent discrimination of global texture orientation. Ordinary threshold for both observers exceeded 3% contrast, nearly six times the contrast required to perform at threshold performance level with first-order textures. This increase in threshold is comparable with other reports of second-order sensitivity (Chubb & Sperling, 1988; Ellemberg, Allen, & Hess, 2004).

As in the first-order task, thresholds initially decrease with increasing amplification then increase as amplifier modulations become very large. Maximal amplification factors of 2.77 and 2.80 were observed with the 16% amplifiers in both observers. Although these values are lower than those observed with first-order textures (Experiment 1), a similar pattern of facilitation is present. Figure 8b illustrates amplification as a function of amplifier modulation depth m_e for the two observers. Again, the classic dipper shaped function can be seen. Amplification factors and RMS energy for the second-order stimuli are listed in Table 2.

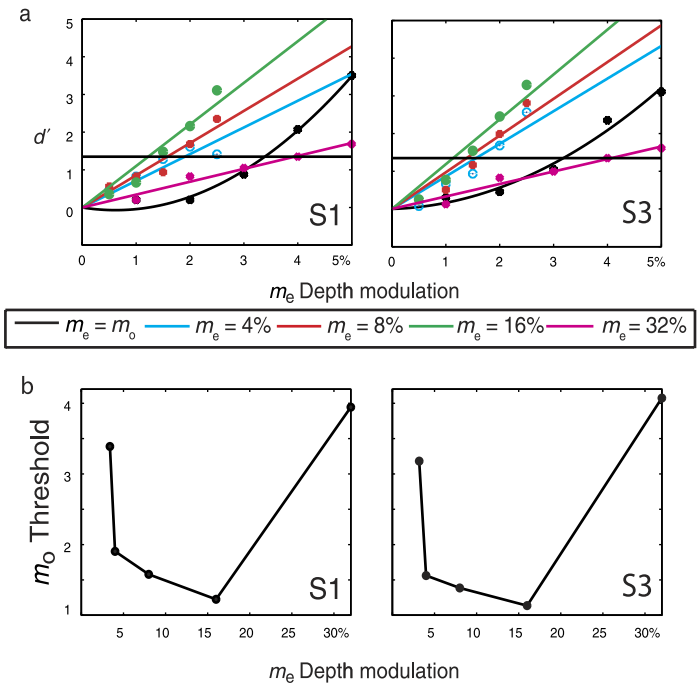

Figure 8. Second-order textures: Accuracy of global orientation discrimination (d') as a function of test stimulus modulation depth m_o for four amplifier modulation depths m_e and for $m_e = m_o$ (ordinary threshold). Data points, psychometric functions, and threshold contrast values for second-order textures conducted with observers S1 and S3 with 2.0 cpd textures (Figures 2d and 2e). (a) d' for global orientation discrimination versus m_o shown in a different color for each amplifier of modulation depth, $m_e = m_o$, 1% 2% 4%, and 8%. (b) Threshold modulation depths m_o for test rows as a function of amplifier modulation depth m_e. The far left point on each graph is the ordinary threshold contrast, values on the curve below ordinary threshold represent contrast amplification. Facilitation in global orientation discrimination in second-order textures is similar to that in first-order textures (compare with Figure 3b).

Subject	Amplifier Contrast	m_e	m_o	Amplification factor	RMS energy
1	$m_e = m_o$	3.39	3.39	1	3.39
m_e = 4%	4	1.9	1.78	2.76	
m_e = 8%	8	1.57	2.15	3.55	
m_e = 16%	16	1.22	2.77	4.43	
m_e = 32%	32	3.95	0.86	11.23	
3	$m_e = m_o$	3.18	3.18	1	3.1818
m_e = 4%	4	1.56	2.04	2.5	
m_e = 8%	8	1.39	2.30	3.33	
m_e = 16%	16	1.14	2.80	4.26	
m_e = 32%	32	4.07	0.78	11.41	

Table 2. Second-order test and amplifier modulations, amplification factors, and stimulus root mean square (RMS) energies.

Global orientation energy based on Fourier analysis

The visual system is believed to extract texture orientation through image convolution with a bank of narrowly tuned filters of different preferred orientations (Freeman, 1989; Knutsson & Granlund, 1983; Landy & Bergen, 1991). These filters, oriented in frequency space, effectively measure power through the Fourier transform of the stimulus. To extract a measure of the oriented Fourier energy, outputs from populations that exhibit different tuning curves must be compared.

Elaborated Reichardt detectors (van Santen & Sperling, 1984) and other equivalent and similar motion energy models (Ahumada & Watson, 1985; Heeger, 1987; Watson & Ahumada, 1985) can be interpreted in terms of the human visual system performing a spatiotemporal Fourier analysis on the incoming visual signal. In the context of motion direction discrimination, such analysis proceeds in two steps (for schematic, see Figure 1b). First a spatiotemporal decomposition is performed on the stimulus. The component outputs of this decomposition are then fed to a decision stage in which a voting rule is applied to decide which direction has the most weight.

In both texture orientation analysis and motion direction analysis, paired quadrature filters act to compute a difference in local Fourier energy (space–space and space–time) of the input image signal and assign a winner to the discrimination. One question we ask is, to what degree do our observed psychophysical results mirror the behavior of such simple Fourier energy detectors?

To test how well simply computing the stimulus' Fourier energy can account for our data, we computed a two-dimensional Fourier analysis of the first-order stimuli using the Matlab FFT2 algorithm. For each stimulus, a discrete Fourier transform was performed on the unpadded, 128 × 128 pixel image, resulting in a two-dimensional matrix of discrete Fourier values, extending to the eighth harmonic of the stimulus and capturing over 99% of the total stimulus power (1.2 cpd = 99.91%, 2.0 cpd = 99.63%, and 2.5 cpd = 99.31%).

As a measure of the oriented energy for each stimulus image, we computed the difference in Fourier values summed over all the orientations from −90° to 0°, subtracted from this sum the energy sum over all orientations from 0° to 90°. This subtraction simulates the operation of quadrature filter pairs (as illustrated in Figure 1b) and produces a phase independent value corresponding to the oriented stimulus energy. We call this difference the oriented Fourier energy difference (oFED).

We test the hypothesis that d' for global orientation discrimination is proportional to the oFED. The constant of proportionality is the reciprocal of the relative efficiency of detection for different amplifier contrasts m_e that is illustrated in Figure 6. Figure 9 depicts d' performance as a function of oFED times efficiency constant for observers S1 and S2 on the main discrimination task over all conditions. Log d' performance is plotted against the log difference in oFED for each of the amplifier values, as indicated by the different colored lines.

Two observations from Figure 9: First, as the difference in oFED increases (holding amplifier row contrast constant), there is a linear increase in d' on the orientation discrimination task. Secondly, stimulus configurations with amplifier rows of contrasts 1%, 2%, and ordinary threshold that have equal oFED also produce nearly equal discrimination performance. This can be seen in the near overlap of points and fits for each of these amplification levels. Texture stimuli containing 4% and 8% amplifier m_e produce significantly worse performance over the range tested.

If the multiplicative property held perfectly, all the functions relating oFED to performance would increase linearly and all curves would fall on top of each other. This would require the RMS threshold energy functions in Figure 6 to be perfectly flat lines. Figure 6 shows that RMS threshold energy obviously declines with for m_e greater than about 2%. The fact that all the d' curves in Figure 9 are fit well by the function $a \times k_e \times$ oFED, where a is a constant across all the conditions and k is the reciprocal of the amplifier efficiency, suggests that once efficiency in different amplifier

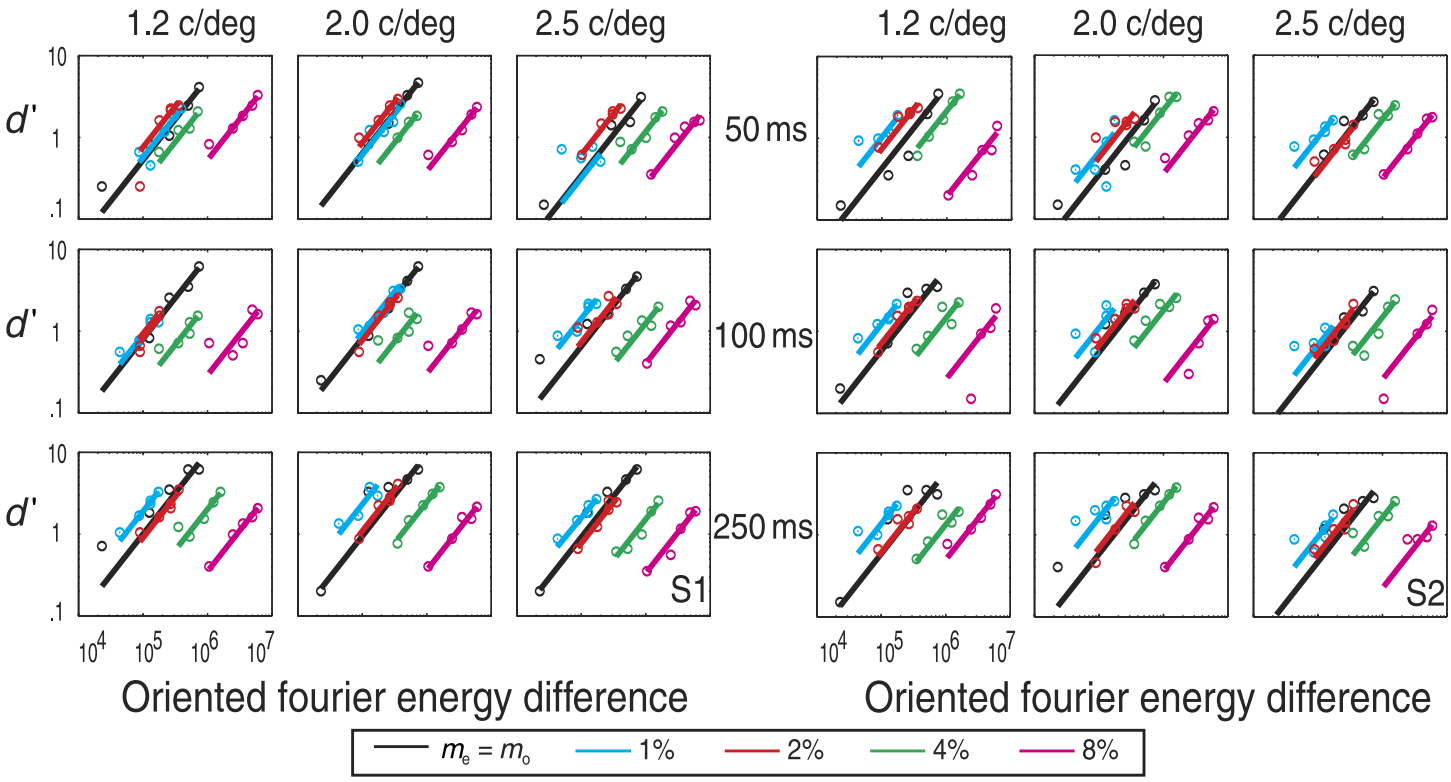

Figure 9. Accuracy of orientation judgments (as a function of the oriented Fourier energy difference (oFED). Ordinate is *d′* on a log scale, the abscissa is the oFED. oFED pools the Fourier components corresponding to the "correct" stimulus orientations, pools "incorrect" stimulus orientations, and subtracts them. The lines through the data represent $a \times k_e \times$ oFED, where *a* is a constant across all the conditions and k_e is the reciprocal of the amplifier efficiency illustrated in Figure 6. Equal Fourier energy produces nearly accuracy, for ordinary threshold, 1% and 2% amplifiers. At higher even row contrasts, efficiency k_e declines.

conditions is accounted for, the multiplicative rule holds and the decrease in efficiency is independent of the computation of orientation. Independence of gain control and the computation of orientation are most logically explained by assuming that the activation of gain control processes (masking) occurs prior to the computation of orientation.

Contrast gain control model

In this section, we show that a simple model (Figure 10) based on the multiplicative principle (Lu & Sperling, 2001a, 2001b; Reichardt, 1961; Van Santen & Sperling, 1984) and feed-forward gain control, via shunting inhibition (Carandini, Heeger, & Movshon, 1997; Foley & Legge, 1981; Lu & Sperling, 1996; Sperling & Sondhi, 1968), accounts for the main results of this study. We further wish to show how the computations for the discrimination of global orientation are naturally embedded in a more comprehensive model of early visual processing. When examined in detail, the microprocesses of global orientation discrimination involve some complexities, but nearly all the complexities are already present in any model that deals more generally with early visual processing. Thus, the schematic representation of the model (Figure 10) contains dead-end arrows that indicate signal flow to other early visual processes beyond the scope of global orientation discrimination.

The schematic representation of the model begins with spatial, orientation selective filters. Although there is an intentional correspondence of these filters with the so-called simple cells of occipital cortex area V1 (e.g., Hubel & Wiesel, 1965; Ringach, Hawken, & Shapley, 2002), the model itself is a purely psychophysical model. For example, in the cortex the representation of a white stripe on a dark background and the representation of a dark stripe on a white background are carried by different V1 simple cells (half-wave rectifiers); in the model, responses to such inputs are simply represented as positive and negative outputs, respectively, of an orientation selective filter. The output of each of the model's orientation selective filters diverges into two paths: A first-order path in which positive and negative signals represent light and dark stripes, respectively, and a second-order path in which the orientation filter outputs are rectified; that is, they yield only positive values that represent the magnitude of a filter's output.

The rectification of filter outputs approximates a squaring (power) function, as illustrated in Figure 11.

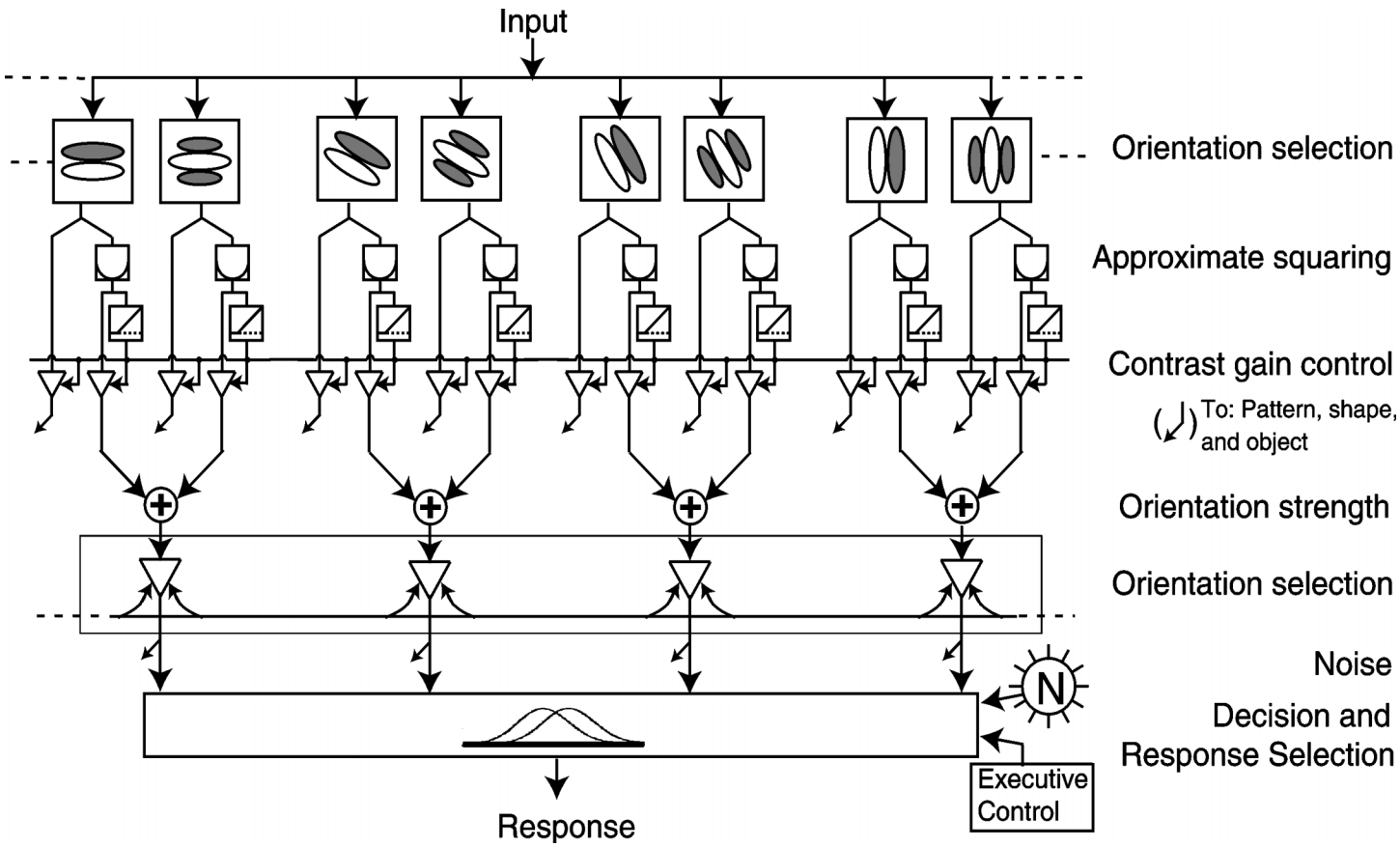

Figure 10. Schematic illustration of a model for visual discrimination of pattern orientation. The visual input is a pixel image. "Orientation selection" indicates an array of band-limited spatial filters that span orientations ranging from 0° to 179°. Each orientation is represented by two filters in a quadrature filter pair, that is, filters differing in phase by 90°. The row "approximate squaring" indicates a power function of the absolute value of the filter output, the exponent of the power function is $2^*\gamma$, where γ is a correction term that is 1.00 for infinitesimal contrasts, is greater than 1 for low contrasts, and asymptotically returns to 1.0 for inputs with contrast amplitudes greater than about 10%. The approximately squared signal splits into two paths. One is subject to a threshold and then applied as "contrast gain control" to all signals, squared and nonsquared. In the other path, the approximately squared signals from the two filters in the quadrature pair are summed to yield orientation strength, which then feeds into orientation selection. Orientation selection restricts the input to the decision and the response stage to the two relevant orientations, the major and the minor (mirror-image) orientations. Executive control is exerted to subtract the magnitudes of these two orientation strength signals, noise is added that represents noise accumulated at all the prior and the present stage, and the response is determined by the sign (+ or −) of the resultant. Arrows that do not end in any illustrated box represent signals that are generated by the processes shown here but are utilized by other perceptual processes.

To represent the function, we use a correction term γ that multiplies the exponent (2) of the square terms in the numerator, causing the net exponent $2^*\gamma$ to be larger than 2 for values of contrast less than 10% and to be nearly equal to 2 for contrast values greater than 10% (Equation 5). This correction term is needed to account for the fact that efficiency (in terms of power, i.e., power law exponent 2) increases with increasing amplifier contrast m_e up to m_e = 2%. There are other possible ways to deal with the fact that, within the framework of this model, square law rectification is only approximately correct. As the current data do not severely constrain the nature of the correction, the γ correction term was used because it is convenient. The approximately squared signal divides into two paths. One path is a gain control path for both first- and second-order orientation signals. The gain control is feed-forward shunting inhibition (Sperling & Sondhi, 1968) with a threshold τ. The second path represents the second-order orientation signal itself, which represents the orientation strength of a particular orientation.

Orientation selection is a competitive process that is modeled here in a simplified form because only two mirror-image orientations are relevant in these experiments. These two fundamental Fourier components essentially contain all the useful Fourier energy of the stimulus. The signals representing the fundamental Fourier components of the two mirror-image orientations are subtracted. The executive processes of understanding the task, selecting the relevant orientations to compare, comparing them via subtraction, and mapping the outcome onto a motor response are represented by the stages of decision and response selection. Internal noise that accrues at all

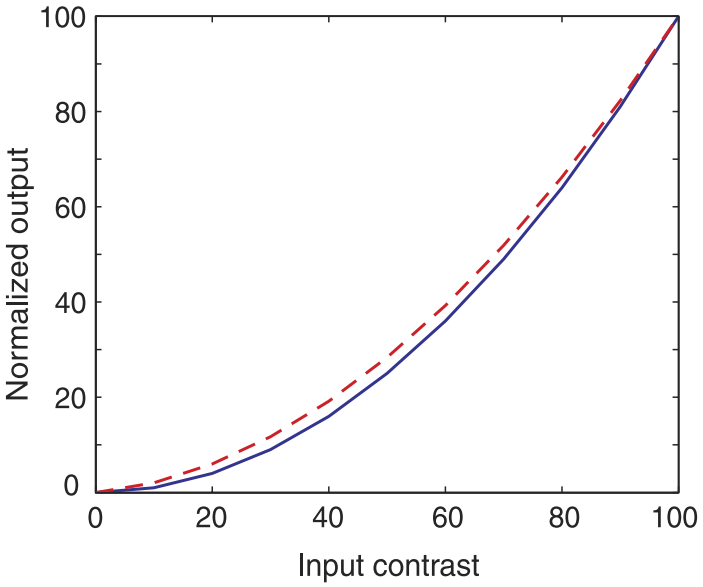

Figure 11. Input output transformations of a pure square and of the approximate square used in the model. The abscissa represents input contrast (0, 1), the ordinate represents the normalized output (0, 1) of the input squared (red, dotted line) and of the approximate square function (blue, solid line) used in the model (Figure 10).

stages of the signal processing is simply represented by the injection of random error at the decision stage. The orientation with the biggest net signal determines the response. The model processes that generate orientation judgments are captured in Equation 4:

$$d' = \frac{\alpha[(m_o + m_e)^{2\gamma} - (m_e - m_o)^{2\gamma}]}{1 + \beta\left\{\max[(m_o + m_e)^{2\gamma} - \tau, 0] + \max[(m_e - m_o)^{2\gamma} - \tau, 0]\right\}}. \quad (4)$$

The numerator of Equation 4 reflects the contrast energy difference of the major and the minor orientations being compared. The denominator of the equation reflects shunting inhibition (Coombs, Eccles, & Fatt, 1955; Sperling & Sondhi, 1968), which is feed-forward gain control exerted by these same contrast energies. The shunting inhibition has a threshold τ that must be surpassed for inhibition to occur. Shunting gain control naturally originates from the mechanisms of neuronal inhibition, as it is divisive gain control as opposed to subtractive inhibition. α and β are scaling parameters of the model: α scales the units of image contrast (i.e., 0, 100%, or 0, 1) and β scales inhibition relative to excitation.

$$\gamma = 1 + \frac{\eta[(m_o + m_e)^2 + (m_e - m_o)^2]}{1 + \lambda^*[|m_e + m_o|^3 + |m_e - m_o|^3]}. \quad (5)$$

Equation 5 describes the correction to the squaring rectification; it contains two estimated parameters. The parameters τ in Equation 4 and η and λ in Equation 5 remain fixed throughout all nine conditions. The parameters α and β vary with condition, reflecting the three different configurations and the three different exposure durations. Thus, to fit all the data for one subject requires $1 + 2 + 9 \times 2 = 21$ parameters. The data to be fit by the model consist of the d' values for each m_o as a function of m_e for each of the three stimulus configurations, times three exposure durations, plus the conventional thresholds measurements, d' as a function of m_o. Data d' values greater than 3.0 were omitted in fitting the model as these data are too unreliable. All in all, there are 214 data points for Observer 1 and 224 points for Observer 2.

A gradient descent procedure that minimized the square difference between the model and measured d' was used to estimate the optimal model parameters. The goodness of fit for each model was determined by

$$r^2 = 1.0 - \frac{\sum \text{sqdiff}}{\sum[d'_{\text{measured}} - \text{mean}(d'_{\text{measured}})]^2}. \quad (6)$$

The model accounts for $r^2 = .905$ of the variance in the data. The model parameters are shown in Table 3, and the model fits are illustrated in Figure 12a. We have also tested a reduced version of the model in which γ was set to be 1.0. The reduced model provided a significantly inferior fit to the data, $r^2 = .7333$, $F(1, 200) = 362.1$, $p < .001$, indicating the need to have the correction to the strict square function in the contrast gain control model. With no new parameters, the model also provides predictions of the threshold odd row contrast modulation m_o for each even row contrast modulation m_e for $d' = 1.0$. These m_o predictions are plotted in Figure 12b. For comparison, using a random 1/2 of the data to predict the other 1/2 of the data would have yielded an r^2 of .851 for Observer 1 and .816 for Observer 2.

Conditions	α	β
50 ms, 1.2 cpd	1.01	0.76
100 ms, 1.2 cpd	0.94	0.71
250 ms, 1.2 cpd	0.71	0.64
50 ms, 2.0 cpd	2.12	2.12
100 ms, 2.0 cpd	2.37	2.11
250 ms, 2.0 cpd	1.50	1.42
50 ms, 2.2 cpd	3.30	2.52
100 ms, 2.2 cpd	4.45	3.34
250 ms, 2.2 cpd	2.55	2.30

Table 3. Reduced model parameters (constants: τ = 1.05; η = 0.95; λ = 0.49).

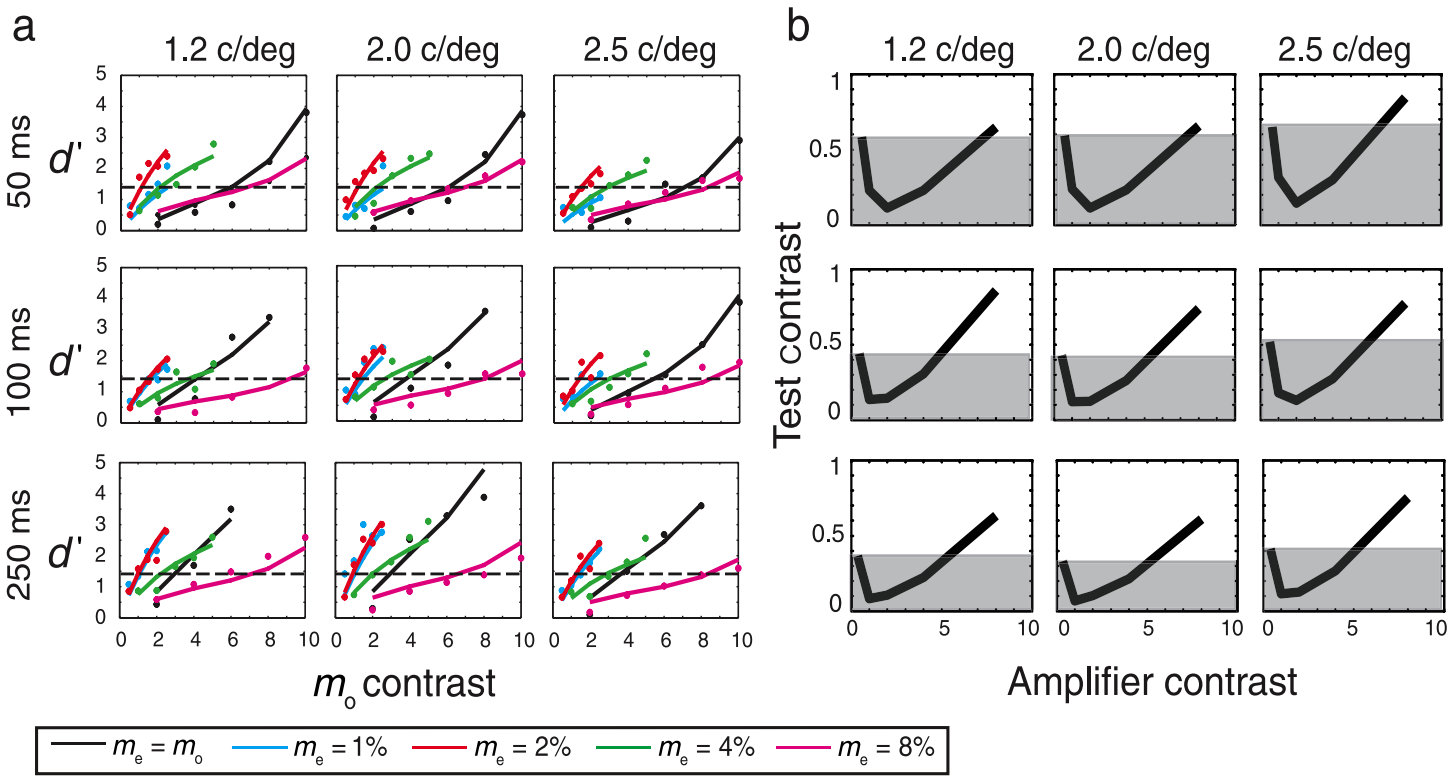

Figure 12. Experimental estimates of the accuracy of global orientation discrimination (d') averaged for the two observers and the model fit to the average data. (a) Observed d' values (points) and model predictions (lines) d' as function of test row contrast m_o for four amplifier row contrasts m_e and for ordinary thresholds $m_e = m_o$ (cf. Figure 4). Three model parameters, λ, η that describe the changing power law exponent, and τ that describe the threshold for gain control, are constant for all nine panels. Two parameters, α and β that describe the strengths of excitation and inhibition (numerator and denominator of Equation 5), are estimated for each stimulus configuration and duration. (b) Model predictions of m_o as a function of m_e for $d' = 1$ (cf. Figure 5).

Applying the model to global orientation discrimination of second-order textures. The model, as expressed in Equations 4 and 5, can be directly applied to account for d' derived from global orientation discrimination in second-order textures. The data for the only second-order texture configuration (Figure 2e) and time (100 ms) tested consist of 25 values of d'. Only the data of observer S1 were sufficiently noise-free to make parameter estimation worthwhile. Five model parameters are required by the Equations 4 and 5; there is no savings by sharing parameters over conditions as only one stimulus configuration and exposure duration was tested. The five-parameter model accounted for 89% of the variance of the second-order data shown in Figure 8a.

Discussion

Main results

In this work, we have demonstrated and quantified contrast amplification through a texture orientation discrimination task. Psychometric functions for forced-choice orientation discrimination showed a classical dipper shape in which pairing below-threshold low-contrast test rows with high-contrast amplifier rows enabled detection of the global texture orientation. Contrast amplification was observed in all participants, was tested on both first- and second-order textures, and was presented over a range of geometries and display durations. Amplification factors greater than 5× were observed for first-order textures, and those greater than 2.5× were observed for second-order textures. Compared with absolute detection thresholds, amplification exceeded 11×. The amplification curves presented in Figure 3b amount to a performance curve for the resolution of texture orientation discrimination. This curve is defined at low contrasts by intrinsic nonamplifiable noise and at high contrasts by contrast gain control mechanisms. The overall shape of the response function is well described by the contrast gain control model provided in Equation 4 for both first- and second-order textures. The overall equation describing the contrast gain control model's response to our stimuli is quite similar in form to equations that have been developed to describe feed-forward gain control

(shunting inhibition) in human psychophysical models (e.g., Lu & Sperling, 1996; Sperling & Sondhi, 1968), gain control in cortical neurons (Carandini et al., 1997; Heeger, 1992; Kapadia, Ito, Gilbert, & Westheimer, 1995), and purely empirical formulations to describe data in discrimination tasks (Foley & Legge, 1981; Legge & Foley, 1980). As was noted, nearly all of the elements of the model are components that are widely believed to be involved in visual processing. What has been added here has been (1) embedding the components for global orientation discrimination within a larger framework of early visual processing, (2) proposing that a nonlinearity more complex than a gain control-modulated power law is required to model visual transduction, and (3) demonstrating that computational model can fit a large data set—more than 200 data points for each observer.

Comparison with other studies

Spatial interaction effects have received considerable attention in the psychophysical literature over practically the entire history of the discipline. It is well accepted that the nature of spatial interactions considerably depends on the specific configuration of the elements under consideration, being either facilitative (reduce detection thresholds) or suppressive (increase detection thresholds) of the perceptual strength of a target stimulus. Visual field eccentricity, contrast, and relative orientation are only a few of the dimension on which interaction effects depend. Two approaches used to characterize spatial interactions are of particular relevance to the findings presented in this paper: the contrasting of discrimination and detection thresholds between colocalized stimuli (referred to as a pedestal task), and measuring changes in detection thresholds in the presence of non-co-localized flankers (termed lateral interaction tasks).

Numerous researchers have shown that the contrast threshold for a test grating is reduced when superimposed on a background (masker) of similar spatial frequency (Olzak & Thomas, 1992; Swift & Smith, 1983; Thomas, Olzak, & Shimozaki, 1992), orientation (Foley & Legge, 1981; Legge & Foley, 1980; Nachmias & Sansbury, 1974; Olzak & Thomas, 1991; Zenger & Sagi, 1996), or phase (Foley & Boynton, 1993). Psychometric functions resulting from these tasks reveal that the difference in intensity threshold for discrimination is substantially lower than the absolute intensity threshold for detection. As observed in our main discrimination task, these findings all show a dip in discrimination thresholds over the range of contrasts closest to detection threshold.

A survey of the magnitude of facilitation effects in spatially colocalized stimuli provides a reference by which to evaluate our amplification factors, presented in Table 1 (or graphically as dippers in Figure 5). Whereas typical ratios of detection to discrimination were under two, results from Nachmias and Sansbury (1974) using unidimensional sine wave gratings of 3 cpd presented for 250 ms reported ratios in the range of two to four. Foley and Legge (1981) found that the contrast which yields 75% correct detection is typically three to four times larger than the difference in contrast that yields 75% correct discrimination for a range of sine wave gratings of spatial frequencies 0.5, 2.0, and 8.0 cpd presented for 100 ms intervals. Whereas particular experimental protocols yielded a considerable range in the facilitatory advantage of discrimination over detection, we know of none larger than those revealed in our data (four to five). One possible explanation of the larger amplification factors observed in the current study is that the contrast gain control signals in our stimuli are weaker than those in typical pedestal experiments—here, only half of the stimulus elements are of high contrast, whereas all the stimulus elements are of high contrast in typical pedestal experiments.

In another related line of research, Polat and Sagi (1993, 1994) demonstrated that the detectability of a low-contrast target grating was strongly influenced (2× threshold decrease) by the presence of a nearby flanking stimuli, with this effect falling off as targets and flankers differs in relative orientation or separation. This form of spatial integration has been proposed as the fundamental basis of contour integration (Field, Hayes, & Hess 1993) and has been replicated and generalized by a number of authors using Gabor stimuli, which are believed to resemble the receptive field profiles of cells in early visual cortex (Chen & Tyler, 2000, 2001, 2002; Williams & Hess, 1998; Zenger & Sagi, 1996; Zenger-Landolt & Koch, 2001). Although it focused on pattern detection, the proposed models of the flank effects (Polat & Sagi, 1994) are remarkably similar to the contrast gain control model in this article.

Uncertainty versus contrast amplification

Although the shifts in psychometric functions toward lower contrasts reported in pedestal and lateral interaction tasks are usually attributed to nonlinear transducer functions, an alternative account of these effects is uncertainty reduction (Pelli, 1985) in the presence of the pedestal or flanks. Recently, Petrov et al. (2006) found that collinear facilitation effects could be largely replicated in the presence of a low-contrast circle surrounding the target and argued that in many designs collinear flankers act as just such a spatial cue, which reduced decision uncertainty rather than amplified the target stimuli.

Given the particular construction of our "sandwich displays," we are in a unique position to contrast the additive effects of lateral interactions with uncertainty reduction effects. Specifically, because successive rows (amplifier or test) are 180° out of phase, they are perfectly ambiguous with regard to the orientation of the global stimulus and the assignment of either orientation is equally possible. Test rows must be *detected* to factor into the *discrimination* of

the texture orientation. It is therefore the case that we have a principled rationale for relating discrimination and detection thresholds both in the presence of amplifier rows (flankers) and in their absence (the control detection task). In the case of the ordinary threshold versus amplified threshold contrast, uncertainty reduction cannot play a role because the task relies on a two-alternate forced-choice design where there is complete uncertainty as to the phase of the test. However, in the case of the amplified threshold versus control detection task, the high-contrast amplifiers could serve as a reference frame by which to reduce uncertainty, therefore accounting for the difference between discrimination amplification factors (4–5×) and detection amplification factors (11×).

As described in the results, amplification factors greater than one (>1) exist in each comparison. Therefore, uncertainty reduction cannot account for all the advantage gained in the amplification. However, for each observer, the discrimination amplification factors are roughly twice as large when contrasted to the detection task. This relative advantage could support the assertion that uncertainty reduction does contribute to spatial facilitation.

Physiological mechanisms

Visual perception is inherently a spatial phenomenon. What is seen at any one point in space is largely dependent upon what is present in neighboring regions of space. Whereas the visual pathway begins with simple localized responses of neurons, some process must link together these local responses to create the contours and textures. Psychophysical models of masking phenomena have been largely inspired by physiological findings describing response properties of early visual cortical neurons (Geisler & Albrecht, 1992; Heeger, 1992; Kapadia et al., 1995).

It is known that the response of a visual cortical neuron to a stimulus presented inside its classically defined receptive field (cRF) can be modulated by stimuli located outside the cRF, in adjacent regions of visual space (for a review, see Albright & Stoner, 2002), and it is generally assumed that flanker facilitation occurs because the receptive field of target mechanisms extends beyond the size of the target. At the same time, facilitation has been shown to be narrowly tuned, with effects dropping off sharply when targets and masks differ by more than a few degrees in orientation, phase, or spatial frequency, suggesting that facilitation is constrained to operate within individual channels (Henning & Wichmann, 2007). In general, broadband inhibition has been suggested as a mechanism that serves to normalize cell responses to avoid response saturation. Such a mechanism would allow cortical neurons to operate within their dynamic range while retaining local population information. Therefore, cortical cells that exhibit both broadband inhibition and orientation selectivity provide a plausible physiological substrate for our psychophysically defined amplification.

The mechanisms of normalization are typically cast in terms of individual units adhering to an accelerating nonlinearity while at the same time being divisively inhibited by a pool of neighboring units (Carandini et al., 1997; Watson & Solomon, 1997). In physiological terms, these mechanisms are usually described as antagonistic center-surround or oriented Gabor receptive fields. It is likely the case that the facilitation observed in our tasks is governed by such mechanisms. One could imagine that the physiological realization of the quadrature decision lies in the difference in paired simple cell receptive fields. Once the texture orientation energy at a particular orientation is computed, the output is passed onto a texture filter in which contrast amplification is carried out. The level of facilitation observed in these tasks likely reflects the optimal tuning of these filters for the textures tested. The particular configuration of amplifier and test row contrasts on any given trial dictates the ratio of straight through excitation, to local pooling of inhibitory sidebands, and in turn the signal-to-noise ratio of the whole neural ensemble. Computations such as gain control and light adaptation occur prior to amplification and thus account for the masking seen at higher amplifier values.

Conclusion

The amplification of subthreshold contrast is a robust phenomenon of texture perception. A display yielding five times amplification enables a grating that would otherwise be 1/5 of the ordinary threshold to determine the perceived orientation of the global configuration in which it is embedded. Further, we find that amplification is consistent over a range of viewing durations and geometries. Our data fit within the theoretical framework of multiplicative amplification derived from motion models and with results demonstrating the facilitation of discrimination over detection as described by pedestal functions.

Acknowledgments

This research was supported by the US Air Force, Life Sciences Directorate, under Grant FA9550-04-1-0225.

Commercial relationships: none.
Corresponding author: Lawrence G. Appelbaum.
E-mail: greg@duke.edu.
Address: B203 Levine Science Research Center PO Box 90999 Durham, NC 27708.

References

Adelson, E. H., & Bergen, J. R. (1985). Spatiotemporal energy models for the perception of motion. *Journal*

of the Optical Society of America A, Optics and image science, 2, 284–299. [PubMed]

Ahumada, A. J., & Watson, A. B. (1985). Equivalent-noise model for contrast detection and discrimination. *Journal of the Optical Society of America A, Optics and image science, 2,* 1133–1139. [PubMed]

Albright, T. D., & Stoner, G. R. (2002). Contextual influences on visual processing. *Annual Review of Neuroscience, 25,* 339–379. [PubMed]

Brainard, D. H. (1997). The Psychophysics Toolbox, *Spatial Vision, 10,* 433–436. [PubMed]

Carandini, M., Heeger, D. J., & Movshon, J. A. (1997). Linearity and normalization in simple cells of the macaque primary visual cortex. *Journal of Neuroscience, 17,* 8621–8644. [PubMed] [Article]

Chen, C. C., & Tyler, C. W. (2000). Spatial long-range modulation of contrast discrimination. *SPIE Proceedings Series, 4080,* 87–93.

Chen, C. C., & Tyler, C. W. (2001). Lateral sensitivity modulation explains the flanker effect in contrast discrimination. *Proceedings of the Royal Society B: Biological Sciences, 268,* 509–516. [PubMed] [Article]

Chen, C. C., & Tyler, C. W. (2002). Lateral modulation of contrast discrimination: Flanker orientation effects. *Journal of Vision, 2*(6):8, 520–530, http://journalofvision.org/2/6/8/, doi:10.1167/2.6.8. [PubMed] [Article]

Chubb, C., & Sperling, G. (1988). Drift-balanced random stimuli: A general basis for studying non-Fourier motion perception. *Journal of the Optical Society of America A, Optics and image science, 5,* 1986–2007. [PubMed]

Coombs, J. S., Eccles, J. C., & Fatt, P. (1955). The specific ionic conductances and the ionic movements across the motoneuronal membrane that produce the inhibitory post-synaptic potential. *The Journal of Physiology, 130,* 326–374. [PubMed] [Article]

Ellemberg, D., Allen, H. A., & Hess, R. F. (2004). Investigating local network interactions underlying first- and second-order processing. *Vision Research, 44,* 1787–1797. [PubMed]

Field, D. J., Hayes, A., & Hess, R. F. (1993). Contour integration by the human visual system: Evidence for a local "association field." *Vision Research, 33,* 173–193. [PubMed]

Foley, J. M., & Boynton, G. M. (1993). Forward pattern masking and adaptation: Effects of duration, interstimulus interval, contrast, and spatial and temporal frequency. *Vision Research, 33,* 959–980. [PubMed]

Foley, J. M., & Legge, G. E. (1981). Contrast detection and near-threshold discrimination in human vision. *Vision Research, 21,* 1041–1053. [PubMed]

Freeman, W. T. A. E. H. (1989). Steerable filters. In *Topical meeting on image understanding and machine vision*. Washington, DC: Optical Society of America.

Geisler, W. S., & Albrecht, D. G. (1992). Cortical neurons: Isolation of contrast gain control. *Vision Research, 32,* 1409–1410. [PubMed]

Hays, W. L. (1988). *Statistics* (4th ed.). Fort Worth, TX: Holt, Rinehart and Winston.

Heeger, D. J. (1987). Model for the extraction of image flow. *Journal of the Optical Society of America A, Optics and image science, 4,* 1455–1471. [PubMed]

Heeger, D. J. (1992). Normalization of cell responses in cat striate cortex. *Visual Neuroscience, 9,* 181–197. [PubMed]

Henning, G. B., & Wichmann, F. A. (2007). Some observations on the pedestal effect. *Journal of Vision, 7*(1):3, 1–15, http://journalofvision.org/7/1/3/, doi:10.1167/7.1.3. [PubMed] [Article]

Hubel, D. H., & Wiesel, T. N. (1965). Receptive fields and functional architecture in two nonstriate visual areas (18 and 19) of the cat. *Journal of Neurophysiology, 28,* 229–289. [PubMed]

Kapadia, M. K., Ito, M., Gilbert, C. D., & Westheimer, G. (1995). Improvement in visual sensitivity by changes in local context: Parallel studies in human observers and in V1 of alert monkeys. *Neuron, 15,* 843–856. [PubMed] [Article]

Knutsson, H., & Granlund, G. H. (1983). *Texture analysis using two-dimensional quadrature filters*. IEEE Computer Society Workshop on Computer Architecture for Pattern Analysis and Image Database Management, Silver Springs, Maryland, IEEE Computer Society.

Landy, M. S., & Bergen, J. R. (1991). Texture segregation and orientation gradient. *Vision Research, 31,* 679–691. [PubMed]

Legge, G. E., & Foley, J. M. (1980). Contrast masking in human vision. *Journal of the Optical Society of America, 70,* 1458–1471. [PubMed]

Lu, Z. L., & Sperling, G. (1996). Contrast gain control in first- and second-order motion perception. *Journal of the Optical Society of America A, Optics, image science, and vision, 13,* 2305–2318. [PubMed]

Lu, Z. L., & Sperling, G. (2001a). Three-systems theory of human visual motion perception: Review and update. *Journal of the Optical Society of America A, Optics, image science, and vision, 18,* 2331–2370. [PubMed]

Lu, Z. L., & Sperling, G. (2001b). Sensitive calibration and measurement procedures based on the amplification principle in motion perception. *Vision Research, 41,* 2355–2374. [PubMed]

Nachmias, J., & Sansbury, R. V. (1974). Letter: Grating contrast: Discrimination may be better than detection. *Vision Research, 14,* 1039–1042. [PubMed]

Naka, K. I., & Rushton, W. A. (1966). S-potentials from luminosity units in the retina of fish (Cyprinidae). *The Journal of Physiology, 185,* 587–599. [PubMed] [Article]

Olzak, L. A., & Thomas, J. P. (1991). When orthogonal orientations are not processed independently. *Vision Research, 31,* 51–57. [PubMed]

Olzak, L. A., & Thomas, J. P. (1992). Configural effects constrain Fourier models of pattern discrimination. *Vision Research, 32,* 1885–1898. [PubMed]

Pelli, D. G. (1985). Uncertainty explains many aspects of visual contrast detection and discrimination. *Journal of the Optical Society of America A, Optics and image science, 2,* 1508–1532. [PubMed]

Pelli, D. G. (1997). The VideoToolbox software for visual psychophysics: Transforming numbers into movies, *Spatial Vision, 10,* 437–442. [PubMed]

Petrov, Y., Verghese, P., & McKee, S. P. (2006). Collinear facilitation is largely uncertainty reduction. *Journal of Vision, 6*(2):8, 170–178, http://journalofvision.org/6/2/8/, doi:10.1167/6.2.8. [PubMed] [Article]

Polat, U., & Sagi, D. (1993). Lateral interactions between spatial channels: Suppression and facilitation revealed by lateral masking experiments. *Vision Research, 33,* 993–999. [PubMed]

Polat, U., & Sagi, D. (1994). The architecture of perceptual spatial interactions. *Vision Research, 34,* 73–78. [PubMed]

Reichardt, W. (1961). Autocorrelation, a principle for the evaluation of sensory information by the central nervous system. In W. A. Rosenblith (Ed.), *Sensory communication* (p. 1961). New York: Wiley.

Ringach, D. L., Hawken, M. J., & Shapley, R. (2002). Receptive field structure of neurons in monkey primary visual cortex revealed by stimulation with natural image sequences. *Journal of Vision, 2*(1):2, 12–24, http://journalofvision.org/2/1/2/, doi:10.1167/2.1.2. [PubMed] [Article]

Sperling, G., & Sondhi, M. M. (1968). Model for visual luminance discrimination and flicker detection. *Journal of the Optical Society of America, 58,* 1133–1145. [PubMed]

Swift, D. J., & Smith, R. A. (1983). Spatial frequency masking and Weber's law. *Vision Research, 23,* 495–505. [PubMed]

Thomas, J. P., Olzak, L. A., Shimozaki, S. S. (1992). Using distinctive Fourier components to discriminate between complex patterns. *Ophthalmic & Physiological Optics, 12,* 189–192. [PubMed]

van Santen, J. P., & Sperling, G. (1984). Temporal covariance model of human motion perception. *Journal of the Optical Society of America A, Optics and image science, 1,* 451–473. [PubMed]

Watson, A. B, & Ahumada, A. J., Jr. (1985). Model of human visual-motion sensing. *Journal of the Optical Society of America A, Optics and image science, 2,* 322–341. [PubMed]

Watson, A. B., & Solomon, J. A. (1997). Model of visual contrast gain control and pattern masking. *Journal of the Optical Society of America A, Optics, image science, and vision, 14,* 2379–2391. [PubMed]

Werkhoven, P., Sperling, G., & Chubb, C. (1994). Perception of apparent motion between dissimilar gratings: Spatiotemporal properties. *Vision Research, 34,* 2741–2759. [PubMed]

Williams, C. B., & Hess, R. F. (1998). Relationship between facilitation at threshold and suprathreshold contour integration. *Journal of the Optical Society of America A, Optics, image science, and vision, 15,* 2046–2051. [PubMed]

Zenger, B., & Sagi, D. (1996). Isolating excitatory and inhibitory nonlinear spatial interactions involved in contrast detection. *Vision Research, 36,* 2497–2513. [PubMed]

Zenger-Landolt, B., & Koch, C. (2001). Flanker effects in peripheral contrast discrimination—Psychophysics and modeling. *Vision Research, 41,* 3663–3775. [PubMed]